



Spectropolarimetric Insight into Plasma Sheet Dynamics of a Solar Flare

Ryan J. French¹ , Philip G. Judge² , Sarah A. Matthews¹ , and Lidia van Driel-Gesztelyi^{1,3,4}

¹ Mullard Space Science Laboratory, University College London, Dorking RH5 6NT, UK

² HAO, National Center for Atmospheric Research, P.O. Box 3000, Boulder CO 80307-3000, USA

³ LESIA, Observatoire de Paris, Université PSL, CNRS, Sorbonne Université, Université Paris Diderot, 5 place Jules Janssen, F-92190 Meudon, France

⁴ Konkoly Observatory of the Hungarian Academy of Sciences, Budapest, Hungary

Received 2019 October 24; revised 2019 November 18; accepted 2019 November 28; published 2019 December 20

Abstract

We examine spectropolarimetric data from the Coronal Multi-channel Polarimeter (CoMP) instrument, acquired during the evolution of the 2017 September 10 X8.2 solar flare on the western solar limb. CoMP captured linearly polarized light from two emission lines of Fe XIII at 1074.7 and 1079.8 nm, from 1.03 to 1.5 solar radii. We focus here on the hot plasma sheet lying above the bright flare loops and beneath the ejected coronal mass ejection. The polarization has a striking and coherent spatial structure, with unexpectedly small polarization aligned with the plasma sheet. By elimination, we find that small-scale magnetic field structure is needed to cause such significant depolarization, and suggest that plasmoid formation during reconnection (associated with the tearing-mode instability) creates magnetic structure on scales below instrument resolution of 6 Mm. We conclude that polarization measurements with new coronagraphs, such as the upcoming Daniel K. Inouye Solar Telescope, will further enhance our understanding of magnetic reconnection and development of turbulence in the solar corona.

Unified Astronomy Thesaurus concepts: Solar magnetic reconnection (1504); Solar flares (1496); Spectropolarimetry (1973); Solar magnetic fields (1503)

1. Introduction

Magnetic reconnection is thought to lie at the heart of energy release in solar flares. The earliest models based upon the dynamics of a planar current sheet (Parker 1957; Sweet 1958) gave rise to slow reconnection rates that depend on the magnetic Lundquist number S by $1/\sqrt{S}$, where $S = v_A L / \eta$. Here, v_A is the Alfvén speed, L the current-sheet half-length, and η the magnetic diffusivity. In the corona, $S \approx 10^{12}$. An alternative magnetohydrodynamic (MHD) model was proposed by Petschek (1964), in which fast steady-state reconnection takes place along a small fraction of the current-sheet length, made possible by the inclusion of slow shocks. Petschek’s model remains of interest as it was the first to yield reconnection rates fast enough to account for the rapid energy release observed in flares, varying instead as $1/\log S$.

These current-sheet configurations were incorporated into the standard “CSHKP” solar flare model (Carmichael 1964; Sturrock 1968; Hirayama 1974; Kopp & Pneuman 1976), where a rising flux rope causes the inflow of oppositely orientated magnetic field lines, creating between them a Sweet–Parker current sheet in which reconnection occurs. The standard model faces well-known fundamental challenges related to plasma microphysics. Petschek’s mechanism assumes a certain large-scale steady configuration, but questions surround how such a configuration might occur (e.g., Kulsrud 2011). Furthermore, additional physics must be introduced to explain how the plasma is heated, and how electric fields capable of accelerating particles to above MeV energies are generated (e.g., Benz 2016).

In recent years, attention has been drawn to the possible role of a tearing-mode instability across current sheets (or plasmoid instability), in explaining the onset of “fast” reconnection, i.e., at a rate independent of S , in various regimes. In MHD, analytical growth rates of the plasmoid instability were derived under conditions where current-sheet lengths greatly exceed their (MHD) thickness (Carbone et al. 1990; Loureiro et al. 2007). Such current sheets were found to be intrinsically

unstable to high-wavenumber perturbations, with growth rates greatly in excess of Alfvén crossing times. A chain of number $S^{3/8}$ ($\approx 10^4$ in the solar corona) plasmoids are formed along sheet length $2L$, each with a length $S^{1/8}$ larger than the current-sheet width $\delta = L/\sqrt{S}$. Numerical 2D simulations with $S = 10^6$ have supported the general picture of disruption of reconnecting current sheets through the plasmoid instability, creating a turbulent cascade with a power spectrum that is consistent with in situ observations of plasma turbulence (Dong et al. 2018). However, theoretical work must still be guided by observations.

In this study, we present observational evidence for the presence of unobservably small magnetic structure that is consistent with the plasmoid-fragmentation picture within a dynamically evolving current sheet in the wake of a coronal mass ejection (CME). We show that the magnitude of linear polarization is sensitive to unresolvable small-scale magnetic structures.

2. The Plasma Sheet Associated with the 2017 September 10 Flare

In the corona, current sheets are predicted to occur with a width of order 10 m (Litvinenko 1996), far below the observable limit of even the best coronal instruments (≈ 200 km). However, rare sheets of hot plasma have been observed, associated with eruptive flares and appearing to be related to reconnection within a current sheet (e.g., Liu 2013). These “plasma sheets” are elusive and notoriously difficult to identify, most readily seen above the solar limb.

Perhaps the brightest and longest-lived plasma-sheet observation to date is associated with an X8.2-class flare on 2017 September 10 (e.g., Cheng et al. 2018; Gary et al. 2018; Kuridze et al. 2019; Li et al. 2018; Long et al. 2018; Longcope et al. 2018; Warren et al. 2018; Morosan et al. 2019). The flare and CME erupted from AR 12673 on the western solar limb, observed across the spectrum by multiple space-based and

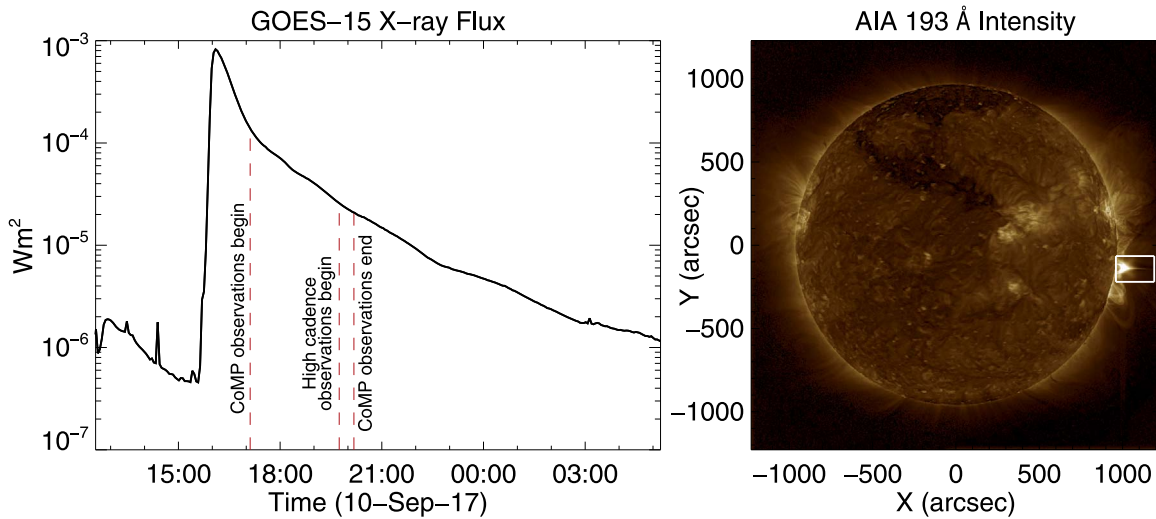


Figure 1. Left panel: GOES-15 X-ray flux for the flare, displaying CoMP observing times. Right panel: location of the plasma-sheet FOV used in this study.

ground-based instruments. Fortuitously, the Coronal Multi-channel Polarimeter (CoMP) instrument obtained polarization data of the plasma sheet, and although the plasma sheet has been well studied, no analysis of its polarized light has been published.

Important earlier studies of intensity images and spectra include that of Warren et al. (2018). They used the Extreme ultraviolet (EUV) Imaging Spectrometer (EIS; Culhane et al. 2007) and Atmospheric Imaging Assembly (AIA; Lemen et al. 2012) data to study the spectroscopic evolution and structure of the plasma sheet. Using temperature-sensitive EIS lines, they calculated a mean plasma-sheet temperature of 15–20 MK. It was deduced that the plasma sheet must be heated by processes originating from magnetic reconnection, as is consistent with the CSHKP model.

Li et al. (2018) and Warren et al. (2018) investigated nonthermal broadening of spectral lines within the plasma sheet, finding nonthermal velocities as high as 200 km s⁻¹. The highest line widths (measuring velocities of plasma superposed along the line of sight (LOS) were seen first at the base of the plasma sheet; later they shifted to higher altitudes. The broad lines were hypothesized to indicate small-scale turbulent velocity fluctuations from plasmoid fragmentation during reconnection. In support of this idea, Cheng et al. (2018) analyzed the plasma-sheet plane-of-sky (POS) outflows and found a power-law spectrum of fluctuations in wavenumber space that is consistent with a turbulent cascade of energy toward smaller scales.

Thus, while there is indirect evidence for the presence of instabilities in the plasma sheet of the 2017 September 10 flare, none of the evidence has provided clear insight into the nature of the plasma sheet’s magnetic field and its role in the onset of turbulence. More direct observations of the magnetic field may be a crucial clue to our understanding magnetic reconnection in this and similar events.

3. Observations

The 2017 September 10 flare originated from AR 12673 on the western limb, peaking at 16:06 UT. In this study we use observations from the High Altitude Observatory CoMP, between 17:07:50 and 20:10:36 UT. The CoMP instrument has an aperture of 20 cm and uses a coronagraph to observe the

low corona from ~ 1.03 to $1.5 R_{\odot}$. CoMP measures the intensity and linear polarization (Stokes I , Q , U) of infrared Fe XIII 1074.7 and 1079.8 nm lines, with a formation temperature of ~ 1.5 MK. 48 of the 62 available observations occurring between 19:44:36 and 20:10:36 UT measured the Fe XIII lines centered at three wavelengths, each through a filter of roughly Gaussian shape (FWHM of 1.3 Å), with a 4.35'' spatial sampling and 30 s cadence. CoMP observing times are shown in the left panel of Figure 1.

The K-Cor instrument at the Mauna Loa Solar Observatory also observed the event, measuring white-light polarization (pB) from 1.05 to $3 R_{\odot}$ over the same observing duration as CoMP. K-Cor has a lower resolution than CoMP (spatial sampling of 5.64'') but a higher cadence of 15 s.

EUV observations by AIA on board the *Solar Dynamics Observatory* provide context, with a higher cadence (~ 12 s) and considerably higher spatial resolution (0.6''). The plasma sheet is most visible in the 193 Å passband, measuring both Fe XXIV and Fe XII emission. Given the plasma sheet’s high temperature, most of the observed emission is likely from the 20 MK Fe XXIV line. Despite its high temperature, the plasma sheet is also seen in cooler AIA passbands, such as 211 Å (Warren et al. 2018), dominated by plasma closer to 2 MK. In AIA 193 Å, the plasma sheet is clearly visible from 16:06 to beyond 20:30 UT. Therefore, although the higher-cadence CoMP observations start 2^h38^m after the flare peak, the plasma sheet is still visible in EUV observations during this time. This is much longer than the Alfvén crossing time, which is just a few minutes for a magnetic field strength of 10 G.

Figure 2(A) shows AIA 193 Å observations of the plasma sheet, averaged over the CoMP observing period and processed using the Multi-Gaussian Normalization technique (Morgan & Druckmüller 2014). In this image, the plasma sheet is seen as the bright horizontal structure, located above the saturated flare loop. A diffraction pattern from saturated intensities is also visible, as a faint cross emanating from the flaring region. The location of this FOV is shown in Figure 1(B).

4. Spectropolarimetry

Linearly polarized radiation is created by the scattering of anisotropic radiation from the solar surface by coronal plasma. The anisotropic radiation generates unequal populations of

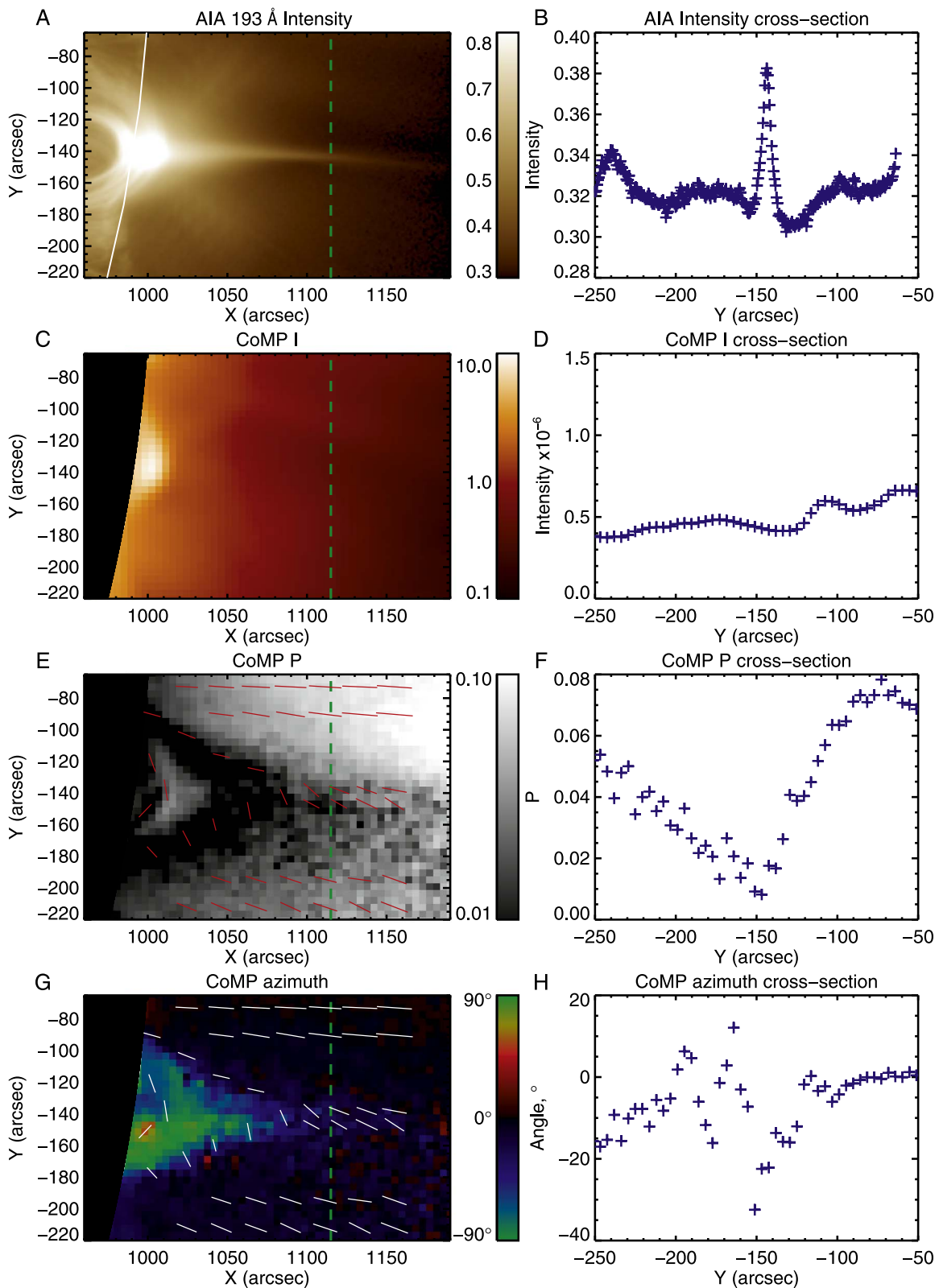


Figure 2. (A) Normalized AIA 193 Å intensity. The curved white line marks the position of the CoMP occulting disk. (B) AIA 193 Å cross-section of intensity along the dashed green line in the adjacent panel. (C) CoMP 1074.7 nm I (D) CoMP 1074.7 nm cross-section of I , along the dashed green line in the adjacent panel. (E) CoMP 1074.7 nm P . Red lines are polarization vectors, with length proportional to $-1/\log(P)$. (F) CoMP 1074.7 nm cross-section of P , along the dashed green line in the adjacent panel. (G) CoMP 1074.7 nm azimuth angle θ , relative to the radial direction. White lines show the corresponding polarization vectors. (H) CoMP 1074.7 nm cross-section of θ , along the dashed green lines in the adjacent panel. CoMP images have an overlaid artificial occulter to increase sharpness at the image edge.

magnetic sub-states (atomic polarization), dependent on the local thermal and magnetic conditions of the plasma (Charvin 1965). The atomic polarization of Fe XIII is, to within a few percent, proportional to the factor $3 \cos^2 \theta_B - 1$, where θ_B is the angle between the magnetic field vector and direction of the center of the incident radiation (Equation (45) of Casini & Judge 1999; Judge 2007). Emission from a complex atom excited by anisotropic radiation must be computed from a solution to the statistical equilibrium equations. The term $3 \cos^2 \theta_B - 1$ is the leading order angular factor in the radiative excitation of atomic sub-levels for each transition. Judge (2007) demonstrated that for multiple levels in an atomic model, the linear polarization arising from sub-level populations follow this term within a few percent for typical M1 transitions. This is because incident solar radiation is strongest in the optical and infrared wavelengths where the M1 transitions are found. The polarization can be destroyed by isotropic processes, including collisions by a sufficiently high density of thermal electrons and protons.

The emitted radiation is linearly polarized by a factor proportional to the amount of atomic polarization, therefore varying as

$$P \propto 3 \cos^2 \theta_B - 1. \quad (1)$$

For a radial magnetic field, the magnetic field vector is parallel to incident radiation ($\theta_B = 0$) and linear polarization is at a maximum. For a tangential magnetic field, atomic polarization becomes negative. The atomic polarization passes through zero as $3 \cos^2 \theta_B = 1$, at the ‘‘Van Vleck’’ angle $\theta_B = \theta_{VV} = 54.74^\circ$. Because we have no prior knowledge of θ_B relative to θ_{VV} , the change in sign of atomic polarization leads to a well-known 90° ambiguity in determining the POS projection of magnetic field direction.

CoMP measures the two components of linear polarization relative to a fixed reference direction, as well as total unpolarized intensity (Stokes U , Q , and I , respectively). Combining these, we calculate fractional linear polarization through

$$P = \sqrt{U^2 + Q^2} / I. \quad (2)$$

We can also use Stokes U and Q to calculate the azimuth angle of the polarization vector in the POS,

$$\theta = \frac{1}{2} \arctan \left(\frac{U}{Q} \right). \quad (3)$$

While θ is determined by U and Q measurements, the corresponding polarization vector has the 90° ambiguity to magnetic field lines, either parallel, perpendicular, or undetermined depending on whether the actual (unknown) angle θ_B is greater than, smaller than, or equal to θ_{VV} . The polarization vector is not a physical ‘‘vector’’ but a line with a magnitude and azimuth.

The corona is optically thin to infrared radiation. Therefore, every observation involves integration over the LOS. Variations in θ_B along the LOS lead to a superposition of different polarization vectors (weighted by the local plasma density), causing a reduction of P .

5. Analysis

Figure 2(A) shows the time-averaged intensity of AIA 193 Å emission, sampling hot Fe XXIV emission, from 18:00-20:00 UT. During this period, the plasma sheet dimmed, but with no significant variation to its shape. The plasma sheet appears as a near-horizontal structure, stretching out from the top of the flare loop arcade ($X \approx 1020''$). A cross-section through the plasma sheet places the plasma-sheet centroid at $Y \approx -145''$ (Figure 2(B)).

In comparison, Figures 2(C) and E, respectively, show intensity I and linear polarization P of cooler Fe XIII 1074.7 nm emission. All CoMP data shown are ‘‘level 2’’ data products from an improved pipeline from early 2019 October (G. de Toma and M. Galloy 2019, private communication).

The images were calculated using the mean of 46 CoMP I , Q , and U measurements from 19:44:36 to 20:03:06 UT (later images were excluded due to poorer seeing from passing cloud). Fe XIII 1074.7 nm emission comes from plasma around ~ 1.5 MK, in contrast to AIA 193 Å at ~ 1.2 and 20 MK. With clear emission in the post-flare loop-top, the absence of strong Fe XIII intensity in the plasma sheet is striking. The AIA 211 and 193 Å channels do show the plasma sheet at the later times CoMP observed, but emission is weaker and more diffuse than at earlier phases.

The fractional linear polarization P reveals a prominent dark triangular structure with a yet smaller dark structure underneath, just above the limb. The latter feature aligns with the bright flare loop-top in the AIA image. The triangular feature however, overlies the bright region over the loop-tops. These two regions both have $P < 0.01$. Above the dark triangular structure, aligned roughly along the AIA plasma-sheet emission, there is a broad, dark region, positioned radially from the top of the overlying structure to the west-most edge of the CoMP FOV. A cross-section through the region shows a significant drop in polarization (Figure 2(F)), despite no clear I signature at the same location (Figure 2(D)). Here, we see a broad gradual drop in polarization down to $P < 0.01$, from values of $P \approx 0.055$ and 0.075 either side of the feature. Despite being ~ 10 times broader than the structure observed in AIA 193 Å, minimum P occurs at approximately the same location as peak AIA 193 Å emission.

Cheng et al. (2018) examined the structure in white light with the K-Cor instrument, measuring the plasma sheet to be 2.5 times larger in polarized brightness (pB) than seen in AIA 193 Å. This difference may be related to the dependencies of EUV and pB intensities on plasma density n as n^2 and n^1 , respectively. Fe XIII emission theoretically depends on n^α , where α is closer to 1 than 2 owing to radiative excitation and some collisional depopulation.

Polarization azimuth angles θ are shown in Figure 2(G). The color map shows angle θ relative to the local radial, and white lines plot the vectors associated with this angle. The plotted vector length is proportional to $-1/\log(P)$. Polarization vectors are also shown in Figure 2(E). The polarization vectors are close to radial above and below the plasma sheet, and apparently trace the outline of the flare loops and overlying magnetic field. Beneath this region, azimuth angles are near tangential to the solar surface. Such behavior is unusual, as azimuth angles normally flip by 90° after crossing $\theta_{VV} \approx 54^\circ$. It can occur under conditions where there is a particular symmetry along the LOS.

Taking a cross-section of polarization azimuths across the sheet, we see the angles moving from -20° to 0° , interrupted

by a large dip to -30° . The peak of the azimuth drop is at the same location as maximum AIA 193 Å emission and minimum Fe XIII polarization. This may be a measurement artifact, as noise in U and Q increase as P decreases.

6. Interpretation

Linear polarization is created throughout the solar corona. There are only two mechanisms by which linear polarization can be reduced. First, collisions by thermal particles can locally destroy atomic polarization. Second, integrations along the LOS and across the POS can both reduce the net polarization observed, dependent on θ_B . At least one of these processes must be responsible for the significant and broad drop in polarization observed across the plasma sheet.

6.1. Collisions

To determine if collisions are responsible for removing polarization in the plasma sheet, we must estimate the density of the region. The CoMP Fe XIII 1074.7 and 1079.8 nm lines are a density-sensitive pair. We used the Coronal Line Emission (CLE) program (Judge & Casini 2001) to determine the relationship between the line intensity ratio and electron density (at 1.5 MK). The 1079.8 nm emission is weak, extending only to the base of the plasma sheet at $\sim 1050''$. At this height, we calculate an electron density at 1.5 MK of $2.8 \times 10^8 \text{ cm}^{-3}$, based on an intensity ratio of 0.27 (Figure 3).

At higher altitudes, this density is likely even lower. We can demonstrate this by measuring the change in total electron density with height, as it is proportional to the polarized brightness pB measured by K-Cor (Figure 3). n_e varies as

$$n_e \approx \frac{\text{pB}}{6.65 \times 10^{-25} 0.11 \ell}, \quad (4)$$

where ℓ is the integration length along the LOS (Orrall et al. 1990).

At an altitude of $1115''$, $\text{pB} = 0.5 \times 10^{-6}$. Therefore, if ℓ is greater than the observed plasma-sheet width $w \approx 5 \text{ Mm}$, $n_e < 1.4 \times 10^{10} \text{ cm}^{-3}$. Assuming $\ell \approx 30 \text{ Mm}$ (Cheng et al. 2018), $n_e \approx 2 \times 10^9 \text{ cm}^{-3}$. These densities are not high enough to destroy atomic polarization via collisions. We therefore conclude that this is unlikely the cause of low linear polarization in the plasma sheet.

6.2. Magnetic Field Structure within the Plasma Sheet

Levels of linear polarization are dependent on magnetic field structure and orientation. The approach of P to zero for angles near $\theta_{\text{Vv}} \approx 54^\circ$ suggests that the small values of P can be accounted for either by a large-scale field close to this angle, or by a more structured field in the POS and/or LOS that contains a mix of angles θ_B .

The morphology of the dark triangular structure in P (Figure 2(E)) strongly suggests that the Van Vleck effect is operating at the edge of the arcade field, as magnetic field lines wrap around the large-scale current systems producing them. Such magnetic null lines are commonly seen in calculations and data (e.g., Judge et al. 2006; Gibson et al. 2017). However, the geometry of a Sweet–Parker plasma sheet, with a magnetic field direction close to radial, is incompatible with continuous Van Vleck nulls produced in this fashion. Such a configuration is shown in Figure 4(A), modeled in CLE as an infinitely long

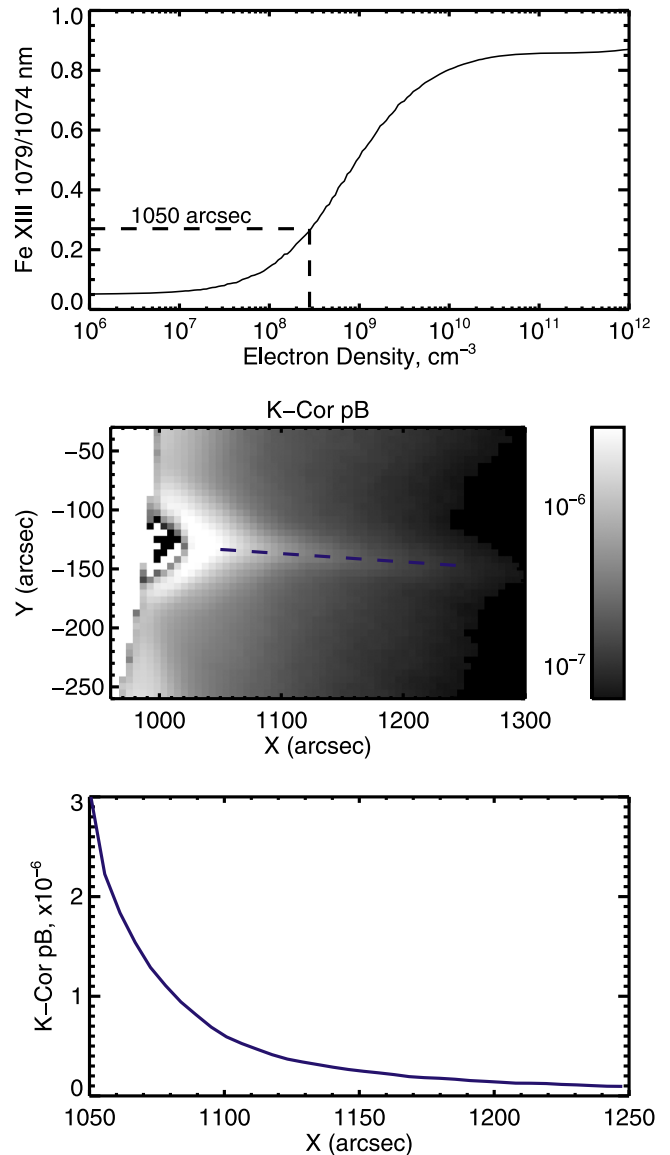


Figure 3. Top panel: theoretical density curve for Fe XIII 1074.7 to 1079.8 nm intensity ratio. The dashed lines mark the measured ratio at $1050''$ above the limb, with corresponding density at this location. Middle panel: time-averaged K-Cor polarized brightness (pB) observations from 18:00–19:30 UT, with units B/B_{sun} . The blue dashed line marks the location of the cross-section in the panel below. Bottom panel: variation in pB along the plasma sheet.

laminar current sheet. Here, we see almost no drop in polarization (Figure 4(B)). Therefore, the levels of P measured by CoMP are inconsistent with a laminar Sweet–Parker current sheet in the standard eruptive flare model.

Small-scale magnetic structures, such as plasmoids or a turbulent magnetic field (formed perhaps as a result of current-sheet instabilities), naturally lead to variations in θ_B . These structures would therefore cause an overall reduction in P , especially if unresolved. To explore such an effect we made simple numerical models using CLE to compare with observations. These simple calculations (Figure 4) show polarization levels P and corresponding polarization vectors. Each case utilizes a similar geometry to CoMP observations, with the plasma sheet centered around the line $y = -0.073x - 67.53$. Sample polarization cross-section profiles are also shown. The models assume that the plasma contributing mostly to the

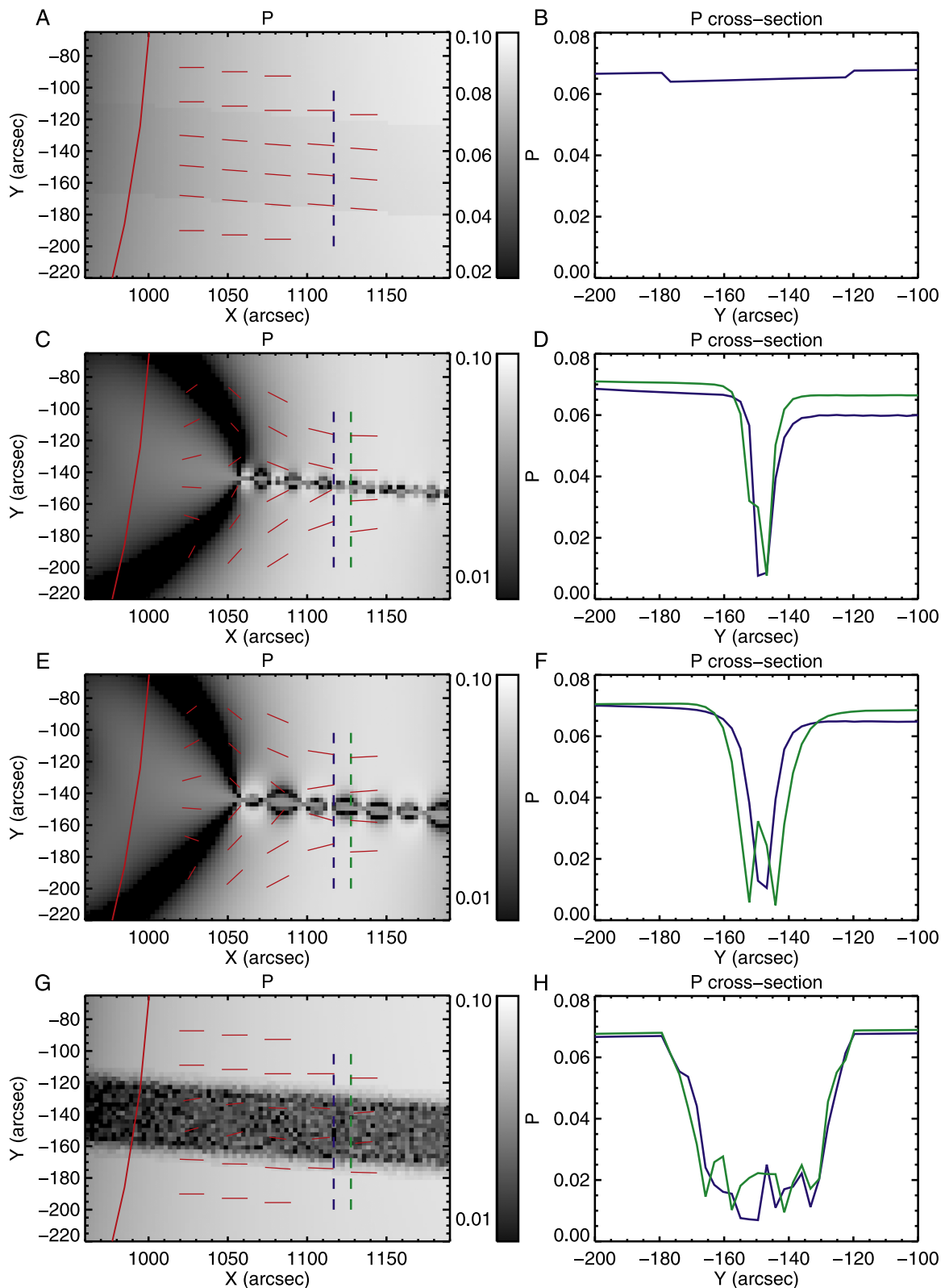


Figure 4. Maps of linear polarization P for plasma-sheet models, with associated cross-sections. CoMP occulting disk position is marked by the red curved line, and polarization vectors as red dashes. Cross-section locations are marked by the blue and green dashed lines, corresponding to the plot color of the cross-section. Models show: (AB) laminar plasma sheet, with magnetic field parallel to the sheet direction. (CD) Potential field model generated from infinite LOS line currents placed at unresolvable intervals along the plasma sheet, combined with a sub-surface dipole. This represents plasmoid reconnection within the current sheet. (EF) The same potential field model as above, but with currents placed at resolvable distances. (GH) Nonphysical plasma sheet with a randomly orientated field, analogous to plasma turbulence.

emission is confined to a narrow region within $10^{-2}R_{\odot}$ of the POS, to avoid LOS cancellations, and thus to highlight effects of POS magnetic structure.

Our “plasmoid” models (Figures 4(C) and (E)) consist of infinite LOS line currents (placed at intervals along the plasma sheet), combined with the potential field generated from a sub-surface dipole. This 2D configuration is the simplest representation of what might constitute a series of magnetic islands formed by the plasmoid instability in the POS.

Figures 4(C) and (E) show calculations of plasmoids with sizes below and above the resolvable limit, respectively. In both cases, the interaction between the plasma-sheet edge and surface dipole form a black “V-shaped” structure, where field lines trace an angle close to the Van Vleck angle. The V shapes occur here as magnetic field lines wrap around the line currents placed along the LOS within the plasma sheet. This is unlikely the cause of the similar structure in CoMP observations, however, as the model relies on the infinite line currents to form this feature. Our primary region of interest is the plasma sheet above this region.

In the unresolvable plasmoid model (Figure 2(C)), polarization drops to a minimum of $P \approx 0.01$ (Figure 2(D)). The resolved plasmoid case (Figure 2(E)) has much more variation in P along the plasma sheet, however, varying greatly between the plasmoid edge and center. In this resolvable case, minimum polarization is calculated as $P \approx 0.005$.

In addition to the plasmoid models, we calculated an unphysical model of a randomly orientated field configuration running along the plasma sheet, again with plasma within $10^{-2}R_{\odot}$ of the POS (Figure 4(G)). Across this structure, we calculate a drop in polarization of to $P \approx 0.015$. In this case, using a random field structure imitates the signal of physical fields which, when integrated over finite volumes, contain the same distribution of vector magnetic fields.

Although these models are relatively simple, they provide an analog for the polarization levels CoMP might observe for representative magnetic topologies. In both the plasmoid and random field cases, magnetic field orientation is shown to be capable of reducing polarization to that observed in this event. With future observations (given an adequate signal-to-noise and integration time), spectropolarimetric measurements can provide observational constraints for the theoretical nature and scale of magnetic substructure in the corona.

7. Discussion

In summary, polarization data from CoMP seem to demonstrate three properties.

1. A broad and gradual reduction of linear polarization across the plasma sheet, with lowest amplitudes at the sheet center.
2. No clear increase in infrared intensity, in contrast with EUV emission.
3. Coherent and large “V-shaped” structures of low polarization below the plasma sheet, reminiscent of the Van Vleck nulls clear in earlier calculations (Judge & Casini 2001).
4. Near-tangential polarization vectors beneath the plasma-sheet, roughly aligned with the aforementioned dark “V-shaped” structures.

The near-tangential polarization seen under the plasma sheet is certainly unusual, as near-radial polarization is found far more frequently (e.g., Arnaud & Newkirk 1987). This is potentially a LOS integration effect through the plasma, canceling out only radial components of polarization. This could perhaps provide information on the large-scale field structure under the plasma sheet, but is an area of future study and does not effect the conclusions drawn in this Letter.

Although our simple plasmoid models can produce the minimum polarization levels observed by CoMP in the 2017 September 10 flare, they do not replicate the gradual and wide drop in the polarization structure, which is significantly broader than EUV observations of the plasma sheet. Recent sophisticated calculations suggest a natural explanation, consistent with the observed behavior of P across the sheet (Stanier et al. 2019). Cascades of plasmoids caused by fragmentation of finer and finer current sheets diffuse from modeled plasma sheets much faster than the plasma itself. We might expect this to produce a similar polarization signature to that observed by CoMP in the later phases of this event. It may also explain in part why the sheet was essentially invisible in the measured Fe XIII intensity, but visible in P . We speculate that if CoMP had started observing at the start of the flare, we would have observed a polarization structure of similar width to observed intensity, broadening as the process calculated by Stanier et al. (2019) evolves.

8. Conclusions





We find that the drop of linear polarization measured by CoMP in the 2017 September 10 flare is consistent with the presence of plasmoids and turbulent fluctuations in the magnetic field. While previous work has focused upon spatially resolvable features in images of the dynamic corona, we have shown that linear polarization can serve as measure for random magnetic structure on sub-resolution scales. Our method provides a diagnostic to analyze the fragmentation of current sheets through the plasmoid instability, which creates a cascade of energy associated with magnetic-field fluctuations toward smaller scales, well below observable limits.

Our work is consistent with theoretical work suggesting the links between current-sheet dynamics, plasmoid fragmentation, and a turbulent cascade of energy associated with magnetic-field fluctuations.

We anticipate that the start of observations with Daniel K. Inouye Solar Telescope will provide data of the necessary quality to further disentangle the intriguing physics discussed here. In particular, a spectrograph (in contrast to the CoMP filtergraph), could further explore the mystery of why P is clearly related to the plasma sheet but I is not.

R.J.F. thanks the STFC for support via funding from the PhD Studentship, as well as NCAR for funding visits to the High Altitude Observatory via the Newkirk Fellowship. The National Center for Atmospheric Research is sponsored by the National Science Foundation. CoMP data services were provided by MLSO. L.v.D.G. and S.A.M. are partially funded under STFC consolidated grant No. ST/S000240/1. The authors would also like to thank Daniel Verscharen for his helpful thoughts on theoretical plasma physics.

ORCID iDs

Ryan J. French  <https://orcid.org/0000-0001-9726-0738>
 Philip G. Judge  <https://orcid.org/0000-0001-5174-0568>
 Sarah A. Matthews  <https://orcid.org/0000-0001-9346-8179>
 Lidia van Driel-Gesztelyi  <https://orcid.org/0000-0002-2943-5978>

References

- Arnaud, J., & Newkirk, G., Jr. 1987, *A&A*, **178**, 263
 Benz, A. O. 2016, *LRSP*, **14**, 2
 Carbone, V., Veltri, P., & Mangeney, A. 1990, *PhFIA*, **2**, 1487
 Carmichael, H. 1964, *NASSP*, **50**, 451
 Casini, R., & Judge, P. G. 1999, *ApJ*, **522**, 524
 Charvin, P. 1965, *AnAp*, **28**, 877
 Cheng, X., Li, Y., Wan, L. F., et al. 2018, *ApJ*, **866**, 64
 Culhane, J. L., Harra, L. K., James, A. M., et al. 2007, *SoPh*, **243**, 19
 Dong, C., Wang, L., Huang, Y.-M., Comisso, L., & Bhattacharjee, A. 2018, *PhRvL*, **121**, 165101
 Gary, D. E., Chen, B., Dennis, B. R., et al. 2018, *ApJ*, **863**, 83
 Gibson, S. E., Dalmasse, K., Rachmeler, L. A., et al. 2017, *ApJL*, **840**, L13
 Hirayama, T. 1974, *SoPh*, **34**, 323
 Judge, P. G. 2007, *ApJ*, **662**, 677
 Judge, P. G., & Casini, R. 2001, in *ASP Conf. Ser.* 236, *Advanced Solar Polarimetry—Theory, Observation, and Instrumentation*, ed. M. Sigwarth (San Francisco, CA: ASP), 503
 Judge, P. G., Low, B. C., & Casini, R. 2006, *ApJ*, **651**, 1229
 Kopp, R. A., & Pneuman, G. W. 1976, *SoPh*, **50**, 85
 Kulsrud, R. M. 2011, *PhPI*, **18**, 111201
 Kuridze, D., Mathioudakis, M., Morgan, H., et al. 2019, *ApJ*, **874**, 126
 Lemen, J. R., Title, A. M., Akin, D. J., et al. 2012, *SoPh*, **275**, 17
 Li, Y., Xue, J. C., Ding, M. D., et al. 2018, *ApJL*, **853**, L15
 Litvinenko, Y. E. 1996, *ApJ*, **462**, 997
 Liu, R. 2013, *MNRAS*, **434**, 1309
 Long, D. M., Harra, L. K., Matthews, S. A., et al. 2018, *ApJ*, **855**, 74
 Longcope, D., Unverferth, J., Klein, C., McCarthy, M., & Priest, E. 2018, *ApJ*, **868**, 148
 Loureiro, N. F., Schekochihin, A. A., & Cowley, S. C. 2007, *PhPI*, **14**, 100703
 Morgan, H., & Druckmüller, M. 2014, *SoPh*, **289**, 2945
 Morosan, D. E., Carley, E. P., Hayes, L. A., et al. 2019, *NatAs*, **3**, 452
 Orrall, F. Q., Rottman, G. J., Fisher, R. R., & Munro, R. H. 1990, *ApJ*, **349**, 656
 Parker, E. N. 1957, *JGR*, **62**, 509
 Petschek, H. E. 1964, *NASSP*, **50**, 425
 Stanier, A., Daughton, W., Le, A., Li, X., & Bird, R. 2019, *PhPI*, **26**, 072121
 Sturrock, P. A. 1968, in *IAU Symp.* 35, *Structure and Development of Solar Active Regions*, ed. K. O. Kiepenheuer (Dordrecht: Reidel), 471
 Sweet, P. A. 1958, in *IAU Symp.* 6, *Electromagnetic Phenomena in Cosmical Physics*, ed. B. Lehnert (Cambridge: Cambridge Univ. Press), 123
 Warren, H. P., Brooks, D. H., Ugarte-Urra, I., et al. 2018, *ApJ*, **854**, 122